Bearing Capacity and Plastic Flow of a Rate-Sensitive Clay under Strip Loading

AUTHOR(S):

MIMURA, Mamoru; SEKIGUCHI, Hideo

CITATION:

MIMURA, Mamoru ...[et al]. Bearing Capacity and Plastic Flow of a Rate-Sensitive Clay under Strip Loading. Bulletin of the Disaster Prevention Research Institute 1986, 36(2): 99-111

ISSUE DATE:

1986-06

URL:

http://hdl.handle.net/2433/124938

Bull. Disas. Prev. Res. Inst., Kyoto Univ., Vol. 36, Part 2, No. 319, June, 1986

Bearing Capacity and Plastic Flow of a Rate-Sensitive Clay under Strip Loading

By Mamoru MIMURA and Hideo SEKIGUCHI

(Manuscript received March 12, 1986)

Abstract

The behavior of a rate-sensitive, saturated clay under strip loading is analysed using the method of finite elements. Emphasis is placed on assessing time effects upon the bearing capacity of such a clay foundation. Computationally, this is made possible by implementing a viscoplastic constitutive model into the analysis procedure and by performing coupled stress-flow analyses with due consideration of the two-phase nature of saturated clay. Loading tests with constant rates of loading as well as those under sustained loads, are treated. It is found that the undrained bearing-capacity factor, N_c, is practically independent of the loading rate despite the significant rate-sensitivities of the bearing capacity and shear strength themselves. It is also found that, within the undrained clay mass undergoing creep under constant loads, there occurs a continued reduction in shear stress with time, and that this stress redistribution prolongs the moment of possible failure under sustained loading much more, as compared with the fictitious situation where the shear stress would remain unchanged. Furthermore, it is shown that partial consolidation during the loading stage exerts profound effects on the migration of effective stress state and on the mobilization of bearing capacity with foundation settlement.

1. Introduction

The bearing capacity of a loaded or excavated clay mass varies significantly with the passage of time. Under unfavorable conditions, the clay mass can undergo eventual failure after the action of embanking or excavation is completed. Such delayed failure obviously merits a due consideration in the construction control for embankments on clay foundations as well as in the design of cut slopes in clay. However, it seems that the governing mechanism has not been fully clarified on a quantitative basis, in any of the four categories of delayed failure illustrated in **Fig. 1.**

This state of the art will be understandable in view of the fact that the process of delayed failure is affected by a number of factors which include the mode and speed of loading, the consolidation history of the clay deposit as well as the physical nature of the constituent soil. In the case of embanking, for example, partial consolidation may be expected to occur in the foundation clay along with contained plastic flow. However, it should be recognized here that the occurrence of partial consolidation does not automatically mean the increase in bearing capacity of the foundation clay, because the partial consolidation is often accompanied by abrupt breakdown in structure of that foundation clay. This aspect is particularly true of highly sensitive, natural clay deposits[1].

The problem of delayed failure becomes even more complicated by the well-known fact that the clay skeleton itself has a marked rate-sensitivity (or intrinsic

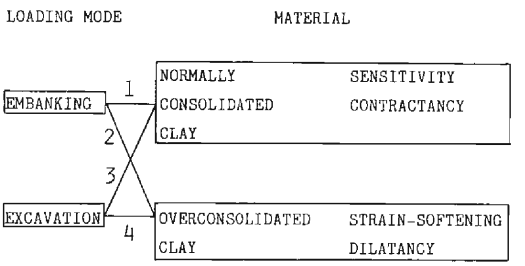

Fig. 1 Factors governing delayed failure.

time effect), as exemplified by creep rupture phenomenon[2].

The present study actually is part of continued research on the whole spectrum of delayed failure illustrated in **Fig. 1**, and will here deal with the specific problem of category 1. Particular emphasis will be placed on clarifying the time-dependent bearing capacity of a rate-sensitive, saturated clay under strip loading, with due consideration of its two-phase nature as well. For this purpose, coupled stress-flow analyses for the clay behavior will subsequently be made using the method of finite elements, after a brief review of a viscoplastic constitutive model to be implemented.

2. A Plane-Strain Viscoplastic Constitutive Model

2.1 Introductory Remark

A viscoplastic constitutive model proposed by Sekighchi[3),4)] is used here to describe the rate-sensitive, plastic behavior of the foundation clay, along with the plane-strain version suggested by Sekiguchi et al.[5]. Note that the plane-strain viscoplastic model is capable of describing the time-dependent stress-strain behavior of normally consolidated clay in a unified manner. Its feature of reproducing the process of undrained creep rupture is particularly important herein, because the aim of the present study lies in critically examining the contribution of such intrinsic time-effect to the so-called delayed failure of a clay mass.

In the next section, the predicted performance of undrained creep rupture will be outlined. For details of the mathematical structure of the viscoplastic model, refer to Appendix I of the present paper.

2.2 Theoretical Features of Undrained Creep Rupture

Let us consider the situation where a K_0-consolidated clay element is subjected to creep loading under undrained plane-strain conditions. Here, K_0 denotes the coefficient of earth pressure at rest. Imagine that the maximum shear stress, $s=\frac{\sigma_1'-\sigma_3'}{2}\left(=\frac{\sigma_1-\sigma_3}{2}\right)$, is instantaneously increased to a prescribed value and then maintained exactly constant with time. Here, σ_1' and σ_3' are the maximum and minimum principal stresses in terms of effective stress, whereas σ_1 and σ_3 denote the maximum and minimum principal stresses in terms of total stress. Then, the plane-

strain viscoplastic model predicts that creep straining is accompanied by the gradual reduction in mean effective stress, $r=\frac{\sigma_1'+\sigma_3'}{2}$. Note that this interesting aspect of undrained creep is a direct consequence of the contractancy (or negative dilatancy) of the clay considered.

Indeed, the imposed, undrained condition for the contractant clay requires the mean effective stress, $r=\frac{\sigma_1'+\sigma_3'}{2}$, to vary with time, t, in the following form:

$$A(r(t))\cdot\exp\left[\frac{-h(r(t))}{\alpha}\right]=\frac{t}{\alpha/\dot{v}_0} \tag{1}$$

Here, $A(r(t))$ and $h(r(t))$ are functions of the mean effective stress $r(t)$, both of which will be defined subsequently. The constants α and $\dot{v}_0$ appearing in Eq. (1), respectively, represent the coefficient of secondary compression and the reference volumetric strain rate.

The failure criterion associated rigorously with the plane-strain viscoplastic model, is expressed as follows:

$$s_f/r_f=\sin\phi' \tag{2}$$

where ϕ' is the angle of internal friction in terms of effective stress and is constant for a given clay. In the creep testing, the value of the shear stress, $s=\frac{\sigma_1'-\sigma_3'}{2}=\frac{\sigma_1-\sigma_3}{2}$, is maintained constant with time. Thus, the value of the mean effective stress, r_f, at creep rupture is expressed as follows:

$$r_f=s_f/\sin\phi'=s_f/\mu \tag{3}$$

where μ stands for $\sin\phi'$.

In view of this relation, the creep rupture life, t_f, can be expressed in the following form:

$$t_f=(\alpha/\dot{v}_0)\cdot A(r_f)\cdot\exp\left[-h(r_f)/\alpha\right] \tag{4}$$

where the values of $A(r_f)$ and $h(r_f)$ are specified by

$$A(r_f)=1-[r_f/r_0]^{\frac{\kappa}{\alpha(1+e_0)}} \tag{5}$$

$$h(r_f)=-\frac{\lambda}{1+e_0}\ln\left(\frac{r_f}{r_0}\right)+\frac{(\lambda-\kappa)}{2(1+e_0)}\ln\left(\frac{\mu^2}{\xi_0^2-\xi_0+\mu}\right)+\frac{(\lambda-\kappa)}{2(1+e_0)\sqrt{\mu-1/4}}\left[\arctan\left(\frac{\mu-1/2}{\sqrt{\mu-1/4}}\right)-\arctan\left(\frac{\xi_0-1/2}{\sqrt{\mu-1/4}}\right)\right] \tag{6}$$

Here, κ is the elastic-compression index, λ the inelastic-compression index, e_0 the initial void ratio, r_0 the initial mean effective stress and ξ_0 the initial value of the effective stress ratio, $\xi=s/r$.

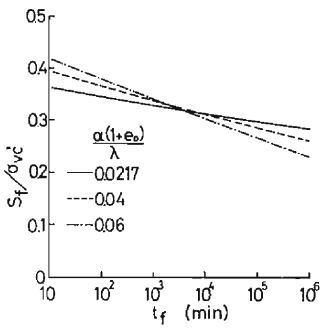

Fig. 2 Relations between creep stress and rupture life.

Table 1 Values of material parameters for Fujinomori clay.

$\lambda=0.115$	$e_0=0.927$
$\kappa=0.0117$	σ'_{v0}*2) $=1.0$ kgf/cm^2
ξ_f*1) $=0.567$	$K_0=0.539$
$\alpha=0.0013$	ξ_0*3) $=0.2995$
$G=120$ kgf/cm^2	$k_0=8.67\times10^{-7}$ cm/min.
$\dot{v}_0=1.3\times10^{-7}$ min.$^{-1}$	$\lambda_k=0.238$

*1) $\xi_f=\sin\phi'$
*2) $\sigma'_{v0}=\sigma'_{vc}$
*3) $\xi_0=(1-K_0)/(1+K_0)$

The features of the derived relation (4) are exemplified in **Fig. 2**, for three different values of the lumped parameter: $\alpha(1+e_0)/\lambda$. The specific value of $\alpha(1+e_0)/\lambda=0.0217$ is selected here for Fujinomori clay, in combination with the values of other parameters given in **Table 1.** The performances of the cases having $\alpha(1+e_0)/\lambda=0.04$ and 0.06 are illustrated for purposes of comparison.

It may be approrpiate here to mention that the development of the shear creep strain, $\gamma=\varepsilon_1-\varepsilon_3$, is clearly related to the evolution of $r(t)$ with time. Indeed, the following relation can be derived for a given constant value of shear stress, s.

$$\gamma(t)=\frac{(s-s_0)}{G}+\frac{\kappa}{1+e_0}\ln\left(\frac{\mu-s/r_0}{\mu-s/r(t)}\right) \qquad (7)$$

Here, s_0 is the value of shear stress at the K_0-consolidation phase prior to the undrained creep considered, and G is the modulus of shear rigidity.

Let us now remember that the value of $r(t)$ for a given time, t, can be determined from Eq. (1). Actually, this equation is a transcendental equation regarding $r(t)$. Therefore, in the present study, the value of $r(t)$for any given value of t is obtained numerically by means of the method of bisection. By substituting thus obtained values of $r(t)$ into Eq. (7), we can construct a shear-creep curve for any given stress system for a given set of material parameters. In **Fig. 3**, two such creep curves are indicated.

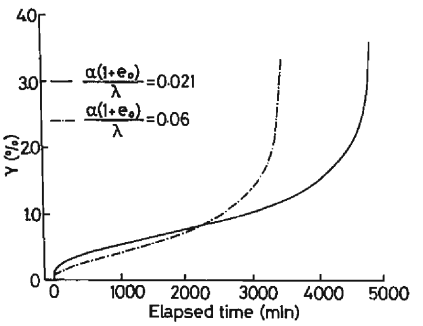

Fig. 3 Relations between creep strain and elapsed time.

The basic creep-rupture characteristics outlined above will serve as a reference of discussion in Chapter 3.

3. Coupled Stress-Flow Analysis in Terms of Finite Elements

3.1 Features of Finite Element Analyses Performed

The stress-strain and strength characteristics of the foundation clay are modelled here by the aforementioned viscoplastic constitutive model. The resulting constitutive relations are implemented into the finite-element analysis procedure through the following incremental form:

$$\{\Delta\sigma'\} = [C^{ep}]\{\Delta\varepsilon\} - \{\Delta\sigma^R\} \tag{8}$$

Here, $\{\Delta\sigma'\}$ and $\{\Delta\varepsilon\}$ are the associated sets of effective stress increments and strain increments, respectively, and $[C^{ep}]$ stands for the elasto-viscoplastic coefficient matrix. The term $\{\Delta\sigma^R\}$ represents a set of "relaxation stresses" which increase with time when strains are held constant.

The pore-water flow is assumed here to obey isotropic Darcy's law. In this connection, it is further assumed that the coefficient of permeability, k, depends on the void ratio, e, in the following form:

$$k = k_0 \cdot \exp\left(\frac{e-e_0}{\lambda_k}\right) \tag{9}$$

Here, k_0 is the initial value of k at $e=e_0$ and λ_k is a material constant governing the rate of change in permeability due to the change in void ratio.

The geometry of the problem to be analysed in this section is shown in **Fig. 4**, together with the finite element mesh used. Note that each quadrilateral element consists of four constant-strain triangles. Also, note that the nodal displacement increments and the element pore-water pressures are taken as the primary unknowns of the problem. The finite element equations governing those unknowns are established on the basis of Biot's formulation[6),7),8)], and are solved numerically by using the semi-band method of Gaussian elimination.

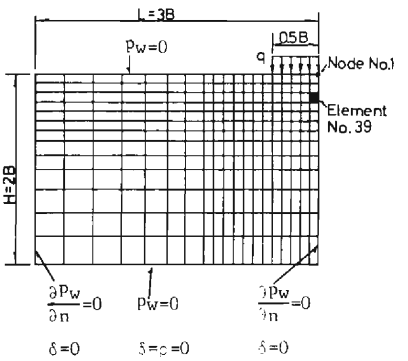

Fig. 4 Finite element mesh with description of boundary conditions imposed.

The width of the loading strip, B, is chosen to be equal to $B=10$ cm, in view of the laboratory model test being undertaken by the authors. The thickness of the foundation clay, H, is selected to be equal to $2B$, whereas the distance from the center line of the loaded area to the lateral boundary, L, is taken as $3B$.

It is assumed that the foundation clay has been normally consolidated under K_0-conditions at a vertical consolidation pressure of $\sigma'_{vc}=1.0$ kgf/cm^2 (98 kPa) for 10^4 minutes, prior to the subsequent loading stage. The values of the material constants as well as those of the initial state variables for the foundation clay, are summarized in **Table 1.**

Three types of loading tests are subsequently analysed, as shown in **Table 2.** Here, $\dot{q}$ denotes the loading rate employed at the constant-rate-of-loading stage. Note that in the case of partially drained loading, the drainage is allowed to occur both from the upper and lower boundaries of the foundation clay, whereas in the

Table 2 Finite element analyses performed.

Drainage condition	Loading mode	Remarks
Undrained	CRL*	$\dot{q}/\sigma'_{vc}=1.25\times10^{-2}$ min.$^{-1}$
		1.04×10^{-3} min.$^{-1}$
		1.04×10^{-4} min.$^{-1}$
	CREEP	$q/\sigma'_{vc}=1.800$
		1.725
		1.650
Partially Drained	CRL*	$\dot{q}/\sigma'_{vc}=1.25\times10^{-2}$ min.$^{-1}$

*CRL=Constant Rate of Loading tests

case of undrained loading, the coefficient of permeability is set equal to zero in the entire region of the foundation clay for computational purposes.

3.2 Results and Discussion

(1) Effect of Loading Rate on Undrained Bearing Capacity

The load-settlement curves obtained at three different loading rates under undrained conditions, are shown in **Fig. 5**, together with the load-settlement curve under partially drained condition. It is seen that, in each of three undrained cases, the foundation clay practically reaches the ultimate state when the dimensionless settlement, ρ/B, becomes equal to 3%. The values of the dimensionless load, q/σ'_{vc}, at the ultimate state are respectively equal to 1.95, 1.875 and 1.8, at the loading rates of $\dot{q}/\sigma'_{vc} = 1.25\times10^{-2}\,\mathrm{min}^{-1}$, $1.04\times10^{-3}\,\mathrm{min}^{-1}$ and $1.04\times10^{-4}\,\mathrm{min}^{-1}$. This means that for this particular problem, the ten-fold change in loading rate gives rise to 4% change of the bearing capacity, q/σ'_{vc}.

The effective stress paths followed by a particular element, No. 39 indicated on **Fig. 4**, are shown in **Fig. 6.** It is seen that the values of the dimensionless shear stress, s/σ'_{vc}, at the ultimate state are respectively equal to 0.346, 0.330 and 0.316, at the loading rates of $\dot{q}/\sigma'_{vc} = 1.25\times10^{-2}\,\mathrm{min}^{-1}$, $1.04\times10^{-3}\,\mathrm{min}^{-1}$ and $1.04\times10^{-4}\,\mathrm{min}^{-1}$. It is of interest here to mention that the bearing capacity factor, N_c, is equal to 5.67 in this particular problem, irrespective of the loading rates imposed.

(2) Effect of Stress Redistribution on Undrained Creep Rate

Let us next consider the performance of undrained creep after the stoppage of the constant rate of loading. The loading speed prior to the creep phase is selected

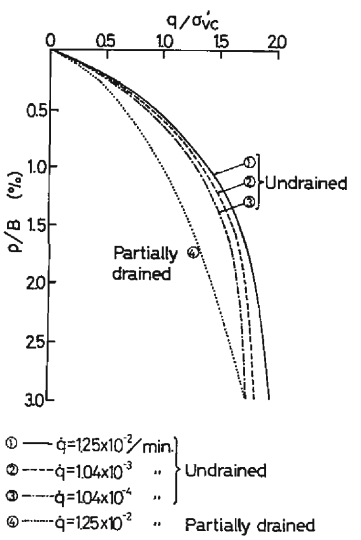

Fig. 5 Load-settlement curves.

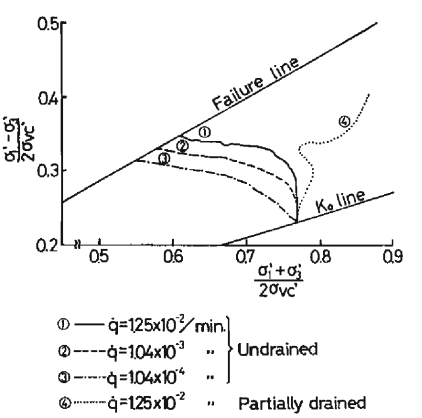

Fig. 6 Effective stress paths followed by a representative soil element.

here to be equal to $\dot{q}/\sigma'_{vc} = 1.25 \times 10^{-2}\,\mathrm{min}^{-1}$. The time-settlement curves for such creep tests at three different values of sustained loads are shown in **Fig. 7.** A line of "failure settlement" given by $\rho/B = 3\%$, is also drawn for purposes of comparison. It is seen that in case C with $q/\sigma'_{vc} = 1.65$, the development of settlement with time is very limited. In case B with $q/\sigma'_{vc} = 1.725$, the settlement is seen to develop at greater rates, as compared with case C. At the highest creep stress of $q/\sigma'_{vc} = 1.8$ (i.e., in case A), the settlement is seen to develop abruptly and exceeds the line of failure settlement in 900 minutes. It should be noted, however, that even in case A with the highest creep stress level, a sign of so-called accelerating creep is not clearly detected.

The evolution of effective stress state during the undrained creep process is shown in **Fig. 8.** It is seen that the effective stress state migrates with time toward the failure line, with the shear stress being gradually reduced. The relations between the final value of the shear stress, s, and the loading time, t, are shown in **Fig. 9.** The results for the aforementioned constant-rate-of-loading tests are also plotted, together with the theoretical s_f versus t_f curve based on Eq. (4). It is seen that the

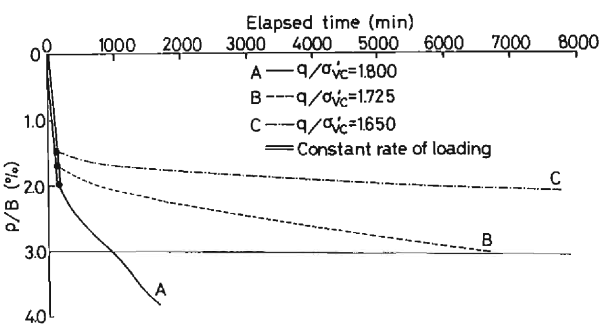

Fig. 7 Time-settlement curves for sustained loading under undrained conditions.

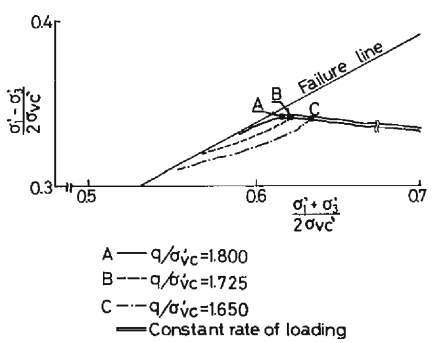

Fig. 8 Effective stress paths followed by a representative soil element, during sustained loading under undrained conditions.

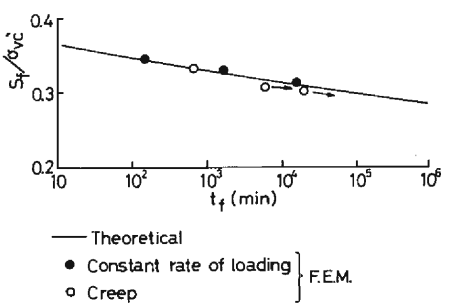

Fig. 9 Shear strengths plotted against durations of loading.

Table 3 Variations in shear stress during sustained loading and the associated variations in rupture life.

Sustained loading test	s/σ'_{vc}	t_f(min.)
A	0.345 → 0.327	138 → 1600
B	0.344 → 0.318	142 → 6500
C	0.343 → 0.311	175 → 20000

results of finite element analyses for the constant-rate-of-loading tests are in good accordance with the theoretical relation. It is also seen that the reduction in shear stress observed in each of the constant-load creep tests has a remarkable consequence upon the occurrence of eventual failure.

In order to see this more clearly, let us here imagine the situation where the shear stress is maintained constant at its initial value. Then, the creep rupture life, t_f, is able to be calculated by Eq. (4), as summarized in **Table 3.**

(3) Effect of Partial Consolidation on the Clay Behavior

The load-settlement curve and a typical effective stress path for partially drained condition have been shown in **Figs. 5** and **6**, with the dotted lines. It is seen from **Fig. 6** that the increase in shear stress is accompanied by a gradual increase in mean effective stress. This behavior is noted to be quite different from those observed for the undrained cases where the mean effective stresses are reduced markedly during the loading stages.

The effect of the partial consolidation on the load-settlement behavior can be seen by comparing curve 4 with curves 1 through 3, all of which are drawn on **Fig. 5.** It is seen that the partial consolidation leads to a slower development of bearing capacity with increasing settlement, and at $\rho/B=3\%$, the partially drained bearing-capacity barely reaches the levels of the undrained bearing capacity.

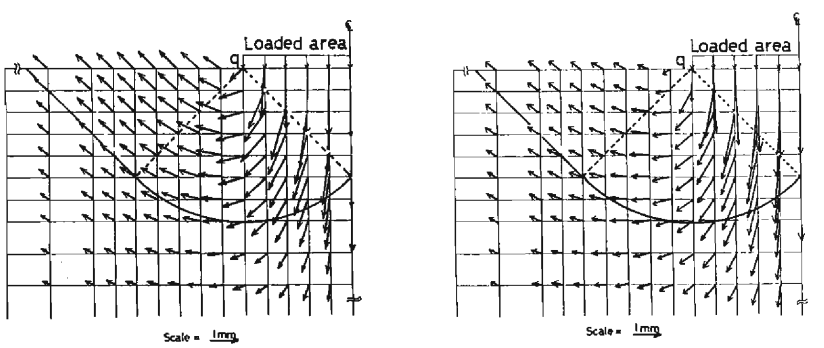

Fig. 10 Displacement vectors at $\rho/B=3\%$:
(a) undrained response
(b) partially drained response

The overall displacement fields, at $\rho/B=3\%$, under partially drained and undrained conditions are compared in **Fig. 10.** The comparison indicates that the partial consolidation tends to suppress the heaving or lateral displacements outside the loaded area. This suggests that the partial consolidation is favorable to the stability of the foundation clay. In this respect, remember the increased effective stresses due to the partial consolidation (**Fig. 6**). It is also to be remarked here that a closer examination of the load-settlement curve for the partially drained case indicates a reduced bearing capacity at a given value of ρ/B (see **Fig. 5**).

In view of the results stated above, it may be concluded that care should be taken in assessing the effect of partial consolidation, as far as the overall performance of the structure-foundation system is concerned.

4. Conclusions

A series of coupled stress-flow analyses for the bearing capacity and plastic flow of a rate-sensitive, saturated clay have been made using the method of finite elements. The principal conclusions drawn from these analyses may be summarized as follows.

1) The undrained bearing capacity of the clay foundation increases with increasing loading rate, in accordance with the associated increase in the shear strength of the clay element. Indeed, the bearing capacity factor, N_c, remains at a practically constant value irrespective of the loading rate.

2) The remarkable redistribution of stress occurs within the foundation clay undergoing creep under constant loads. This phenomenon prolongs the moment of possible failure of the foundation clay much more, as compared with the fictitious case where the shear stress in the soil mass would have been maintained constant during the creep process.

3) The occurrence of the partial consolidation during the loading stage is favorable to the stability of the foundation clay itself. However, it should be kept in mind that such partial consolidation is accompanied by a remarkable increase in settlement at a given load, as compared with the undrained loading. Therefore, the assessment of the effect of partial consolidation should be made regarding the overall performance of the structure-foundation system.

Acknowledgements

The authors wish to express their sincere gratitude to Prof. Toru Shibata, who gave much valuable advice and encouragement during the course of this study. Thanks are extended to Dr. Atsushi Yashima for his helpful discussion. The assistance of Mr. Hiroki Shimizu in the drawing up of diagrams in this paper is greatly appreciated.

All the computations reported in this paper were performed at the Data Processing Center, Kyoto University.

Appendix I. Theoretical Features of Two Viscoplastic Models

The theoretical features of the viscoplastic model proposed by Sekiguchi as well as those of its plane strain version, are summarized in **Table A-1.** Note that the superscript, p, is used here to identify the viscoplastic component of any physical quantity. Also, note that the dilatancy function $g(\xi)$ in the plane-strain version has been specified by

$$g(\xi) = \frac{(\lambda-\kappa)}{2(1+e_0)} \ln\left(\frac{\xi^2-\xi+\mu}{\xi_0^2-\xi_0+\mu}\right) + \frac{(\lambda-\kappa)}{2(1+e_0)\sqrt{\mu-1/4}}\left[\arctan\left(\frac{\xi-1/2}{\sqrt{\mu-1/4}}\right)-\arctan\left(\frac{\xi_0-1/2}{\sqrt{\mu-1/4}}\right)\right] \quad \text{(A-1)}$$

where ξ denotes the stress ratio, s/r and ξ_0 stands for its initial value.

It is evident from **Table A-1** that the mathematical structure of each model is essentially the same. A principal difference lies in that, as its name implies, the

Table A-1 Features of two viscoplastic models.

Subject	Sekiguchi (1977)	Plane-strain version (1982)
1) Viscoplastic flow rule	$\dot{\varepsilon}_{ij}^{\,p}=\Lambda\dfrac{\partial F}{\partial \sigma_{ij}'}$	
2) Viscoplastic potential	$F=\alpha\cdot\ln\left[1+\dfrac{\dot{v}_0\cdot t}{\alpha}\exp\left(\dfrac{f}{\alpha}\right)\right]=v^p$	
3) Consistency condition	$\dot{F}=\dfrac{\partial F}{\partial \sigma_{ij}'}\cdot\dot{\sigma}_{ij}'+\dfrac{\partial F}{\partial t}=\dot{v}^p$	
4) "Static" yield function	$f=\dfrac{\lambda-\kappa}{1+e_0}\ln\left(\dfrac{p}{p_0}\right)+D\cdot\left(\dfrac{q}{p}-\dfrac{q_0}{p_0}\right)$ where $p=\dfrac{1}{3}\sigma_{ii}'$, $q=\sqrt{\dfrac{3}{2}s_{ij}s_{ij}}$ $(i,j=1,3)$	$f=\dfrac{\lambda-\kappa}{1+e_0}\ln\left(\dfrac{r}{r_0}\right)+g\left(\dfrac{s}{r}\right)$ where $r=\dfrac{1}{2}\sigma_{ii}'$, $s=\sqrt{\dfrac{1}{2}s_{ij}s_{ij}}$ $(i,j=1,2)$
5) Strain-rate parameters	$\dot{\varepsilon}^p/\dot{v}^p=\dfrac{1}{M-q/p}$ where * $\dot{\varepsilon}^p=\dfrac{2}{3}(\dot{\varepsilon}_1^{\,p}-\dot{\varepsilon}_3^{\,p})$, $\dot{v}^p=\dot{\varepsilon}_1^{\,p}+\dot{\varepsilon}_2^{\,p}+\dot{\varepsilon}_3^{\,p}$	$\dot{\gamma}^p/\dot{v}^p=\dfrac{s/r}{\sin\phi'-s/r}$ where $\dot{\gamma}^p=\dot{\varepsilon}_1^{\,p}-\dot{\varepsilon}_3^{\,p}$, $\dot{v}^p=\dot{\varepsilon}_1^{\,p}+\dot{\varepsilon}_3^{\,p}$

* For the purpose of illustration the particular expression valid for axisymmetric strain conditions ($\dot{\varepsilon}_2^{\,p}=\dot{\varepsilon}_3^{\,p}$) is listed here.

plane-strain version is based on the two-dimensional stress parameters, r and s, instead of their counterpart, p and q. Another point to be made here is that the plane-strain version leads to generally better predictions for K_0-values; this is a direct consequence of the specific relation between $\dot{\gamma}^p/\dot{v}^p$ and $\xi(=s/r)$ indicated in **Table A-1.**

Appendix II. Notation

B	width of strip loading
D	coefficient of dilatancy
e_0	initial void ratio
G	elastic shear modulus
H	thickness of clay layer
k	coefficient of permeability
L	distance to lateral boundary
M	effective stress ratio at critical state
N_c	bearing capacity factor
q	load intensity
$\dot{q}$	loading rate
r	mean effective stress defined by $r=(\sigma_1'+\sigma_3')/2$
s	maximum shear stress defined by $s=(\sigma_1'-\sigma_3')/2$
t	elapsed time
t_f	rupture life
v^p	viscoplastic volumetric strain
$\dot{v}^p$	viscoplastic volumetric strain rate
$\dot{v}_0$	reference volumetric strain rate
α	secondary compression index
γ	maximum shear strain $(\varepsilon_1-\varepsilon_3)$
ε_1, ε_3	principal strains
κ	swelling index
λ	compression index
μ	effective stress ratio at critical state in the plane strain condition
ξ	effective stress ratio defined by $\xi=s/r$
ρ	settlement at center of loaded area
σ_1, σ_3	principal stresses in terms of total stress
σ_1', σ_3'	principal stresses in terms of effective stress
σ_{vc}'	consolidation pressure
ϕ'	friction angle in terms of effective stress

References

1) Leroueil, S., F. Tavenas, F. Brucy, P. La Rochelle and M. Roy: Behavior of Destructured Natural Clays, Journal of the Geotechnical Engineering Division, ASCE, Vol. 105, No. GT6, 1979, pp. 759–778.

2) Casagrande, A. and S.D. Wilson: Effect of Rate of Loading on the Strength of Clays and Shales at Constant Water Content, Geotechnique, Vol. 2, 1951, pp. 251–263.
3) Sekiguchi, H.: Rheological Characteristics of Clays, Proc. 9th ICSMFE, Tokyo, Vol. 1, 1977, pp. 289–292.
4) Sekiguchi, H.: Theory of Undrained Creep Rupture on Normally Consolidated Clay Based on Elasto-Viscoplasticity, Soils and Foundations, Vol. 24, No. 1, 1984, pp. 129–147.
5) Sekiguchi, H., Y. Nishida and F. Kanai: A Plane-Strain Viscoplastic Constitutive Model for Clay, Proc. 37th Nat. Conf., JSCE, 1982, pp. 181–182 (in Japanese).
6) Christian, J.T.: Undrained Stress Distribution by Numerical Methods, Journal of the Soil Mechanics Foundation Division, ASCE, Vol. 94, No. SM6, 1968, pp. 1333–1345.
7) Akai, K. and T. Tamura: An Application of Nonlinear Stress-Strain Relations to Multi-Dimensional Consolidation Problems, Annuals, Disas. Prev. Res. Inst., Kyoto University, No. 21 B-2, 1976, pp. 19–35 (in Japanese).
8) Shibata, T. and H. Sekiguchi: A Method of Predicting Failure of Embankment Foundation Based on Elasto-Viscoplastic Anlayses, Proc. of JSCE, No. 301, 1980, pp. 93–104 (in Japanese).